Research Article | Vol. 25, No. 4 | 20 Feb 2017 | OPTICS EXPRESS 3124

Optics EXPRESS

Photonic crystal waveguides on silicon rich nitride platform

KAPIL DEBNATH,[1,*] THALIA DOMINGUEZ BUCIO,[2] ABDELRAHMAN AL-ATTILI,[1] ALI Z. KHOKHAR,[2] SHINICHI SAITO,[1] AND FREDERIC Y. GARDES[2]

[1]*Faculty of Physical Sciences and Engineering, University of Southampton, Southampton SO17 1BJ, UK*
[2]*Optoelectronics Research Centre, University of Southampton, Southampton SO17 1BJ, UK*
[*]*K.Debnath@soton.ac.uk*

Abstract: We demonstrate design, fabrication, and characterization of two-dimensional photonic crystal (PhC) waveguides on a suspended silicon rich nitride (SRN) platform for applications at telecom wavelengths. Simulation results suggest that a 210 nm photonic band gap can be achieved in such PhC structures. We also developed a fabrication process to realize suspended PhC waveguides with a transmission bandwidth of 20 nm for a W1 PhC waveguide and over 70 nm for a W0.7 PhC waveguide. Using the Fabry–Pérot oscillations of the transmission spectrum we estimated a group index of over 110 for W1 PhC waveguides. For a W1 waveguide we estimated a propagation loss of 53 dB/cm for a group index of 37 and for a W0.7 waveguide the lowest propagation was 4.6 dB/cm.

OCIS codes: (130.5296) Photonic crystal waveguides; (230.5298) Photonic crystals; (130.0130) Integrated optics.

References and links

1. K. Debnath, K. Welna, M. Ferrera, K. Deasy, D. G. Lidzey, and L. O'Faolain, "Highly efficient optical filter based on vertically coupled photonic crystal cavity and bus waveguide," Opt. Lett. **38**(2), 154–156 (2013).
2. H. C. Nguyen, Y. Sakai, M. Shinkawa, N. Ishikura, and T. Baba, "10 Gb/s operation of photonic crystal silicon optical modulators," Opt. Express **19**(14), 13000–13007 (2011).
3. K. Debnath, L. O'Faolain, F. Y. Gardes, A. G. Steffan, G. T. Reed, and T. F. Krauss, "Cascaded modulator architecture for WDM applications," Opt. Express **20**(25), 27420–27428 (2012).
4. A. A. Liles, K. Debnath, and L. O'Faolain, "Lithographic wavelength control of an external cavity laser with a silicon photonic crystal cavity-based resonant reflector," Opt. Lett. **41**(5), 894–897 (2016).
5. M. G. Scullion, A. Di Falco, and T. F. Krauss, "Slotted photonic crystal cavities with integrated microfluidics for biosensing applications," Biosens. Bioelectron. **27**(1), 101–105 (2011).
6. W. C. Lai, S. Chakravarty, Y. Zou, and R. T. Chen, "Silicon nano-membrane based photonic crystal microcavities for high sensitivity bio-sensing," Opt. Lett. **37**(7), 1208–1210 (2012).
7. A. Faraon, I. Fushman, D. Englund, N. Stoltz, P. Petroff, and J. Vučković, "Coherent generation of non-classical light on a chip via photon-induced tunnelling and blockade," Nat. Phys. **4**(11), 859–863 (2008).
8. A. H. Safavi-Naeini, J. Chan, J. T. Hill, T. P. M. Alegre, A. Krause, and O. Painter, "Observation of quantum motion of a nanomechanical resonator," Phys. Rev. Lett. **108**(3), 033602 (2012).
9. B. Corcoran, C. Monat, C. Grillet, D. J. Moss, B. J. Eggleton, T. P. White, L. O'Faolain, and T. F. Krauss, "Green light emission in silicon through slow-light enhanced third-harmonic generation in photonic-crystal waveguides," Nat. Photonics **3**(4), 206–210 (2009).
10. C. Monat, C. Grillet, M. Collins, A. Clark, J. Schroeder, C. Xiong, J. Li, L. O'Faolain, T. F. Krauss, B. J. Eggleton, and D. J. Moss, "Integrated optical auto-correlator based on third-harmonic generation in a silicon photonic crystal waveguide," Nat. Commun. **5**, 3246 (2014).
11. M. Notomi, K. Yamada, A. Shinya, J. Takahashi, C. Takahashi, and I. Yokohama, "Extremely large group-velocity dispersion of line-defect waveguides in photonic crystal slabs," Phys. Rev. Lett. **87**(25), 253902 (2001).
12. Y. A. Vlasov, M. O'Boyle, H. F. Hamann, and S. J. McNab, "Active control of slow light on a chip with photonic crystal waveguides," Nature **438**(7064), 65–69 (2005).
13. D. M. Beggs, T. P. White, L. O'Faolain, and T. F. Krauss, "Ultracompact and low-power optical switch based on silicon photonic crystals," Opt. Lett. **33**(2), 147–149 (2008).
14. D. M. Beggs, I. H. Rey, T. Kampfrath, N. Rotenberg, L. Kuipers, and T. F. Krauss, "Ultrafast tunable optical delay line based on indirect photonic transitions," Phys. Rev. Lett. **108**(21), 213901 (2012).
15. C. Monat, M. Ebnali-Heidari, C. Grillet, B. Corcoran, B. J. Eggleton, T. P. White, L. O'Faolain, J. Li, and T. F. Krauss, "Four-wave mixing in slow light engineered silicon photonic crystal waveguides," Opt. Express **18**(22), 22915–22927 (2010).

#279245 https://doi.org/10.1364/OE.25.003214
Journal © 2017 Received 20 Oct 2016; revised 5 Dec 2016; accepted 5 Dec 2016; published 7 Feb 2017

Optics EXPRESS

16. C. Monat, M. Ebnali-Heidari, C. Grillet, B. Corcoran, B. J. Eggleton, T. P. White, L. O'Faolain, J. Li, and T. F. Krauss, "Four-wave mixing in slow light engineered silicon photonic crystal waveguides," Opt. Express **18**(22), 22915–22927 (2010).
17. X. Checoury, M. El Kurdi, Z. Han, and P. Boucaud, "Enhanced spontaneous Raman scattering in silicon photonic crystal waveguides on insulator," Opt. Express **17**(5), 3500–3507 (2009).
18. J. Leuthold, C. Koos, and W. Freude, "Nonlinear silicon photonics," Nat. Photonics **4**(8), 535–544 (2010).
19. D. J. Moss, R. Morandotti, A. L. Gaeta, and M. Lipson, "New CMOS-compatible platforms based on silicon nitride and Hydex for nonlinear optics," Nat. Photonics **7**(8), 597–607 (2013).
20. L. Zhang, A. M. Agarwal, L. C. Kimerling, and J. Michel, "Nonlinear Group IV photonics based on silicon and germanium: from near-infrared to mid-infrared," Nanophotonics **3**(4–5), 247–268 (2014).
21. S. Minissale, S. Yerci, and L. Dal Negro, "Nonlinear optical properties of low temperature annealed silicon-rich oxide and silicon-rich nitride materials for silicon photonics," Appl. Phys. Lett. **100**(2), 021109 (2012).
22. C. J. Krückel, A. Fülöp, T. Klintberg, J. Bengtsson, P. A. Andrekson, and V. Torres-Company, "Linear and nonlinear characterization of low-stress high-confinement silicon-rich nitride waveguides," Opt. Express **23**(20), 25827–25837 (2015).
23. C. Lacava, S. Stankovic, A. Khokhar, T. Dominguez, F. Gardes, D. J. Richardson, G. T. Reed, and P. Petropoulos, "CMOS-compatible silicon-rich nitride waveguides for ultrafast nonlinear signal processing," in *Proc. CLEO* (2016), paper STu4Q–7.
24. T. Wang, T. D. K. Ng, S. K. Ng, Y. T. Toh, A. K. L. Chee, G. F. Chen, Q. Wang, and D. T. Tan, "Supercontinuum generation in bandgap engineered, back-end CMOS compatible silicon rich nitride waveguides," Laser Photonics Rev. **9**(5), 498–506 (2015).
25. T. Domínguez Bucio, A. Z. Khokhar, C. Lacava, S. Stankovic, G. Z. Mashanovich, P. Petropoulos, and F. Y. Gardes, "Material and optical properties of low-temperature NH_3-free PECVD SiN_x layers for photonic applications," J. Phys. D Appl. Phys. **50**(2), 025106 (2017).
26. J. P. Hugonin, P. Lalanne, T. P. White, and T. F. Krauss, "Coupling into slow-mode photonic crystal waveguides," Opt. Lett. **32**(18), 2638–2640 (2007).
27. C. Y. Lin, X. Wang, S. Chakravarty, B. S. Lee, W. C. Lai, and R. T. Chen, "Wideband group velocity independent coupling into slow light silicon photonic crystal waveguide," Appl. Phys. Lett. **97**(18), 183302 (2010).

1. Introduction

A strong light-matter interaction between the optical field and the material medium is essential for a diverse field of applications, ranging from integrated photonics, optical sensing, quantum optics, and nonlinear optics etc. Two-dimensional Photonic Crystals (PhC) offer such strong interaction due to their ability to confine light in a tiny space or to control the speed of light [1–10]. It has been well established now that by using the slow light property of PhC waveguides, light can be propagated through them at a fraction of the speed of light in vacuum [11,12]. This ability of PhC waveguides has been exploited for many linear or nonlinear applications, such as electro-optic modulation [2] and optical switching [13], optical delay line [14], signal regeneration through four wave mixing [15,16] and Raman amplification [17] etc. Silicon-on-insulator (SOI) has always been the most preferred material for such demonstrations with PhC structures for telecomm wavelengths, primarily because of two reasons: first, Si-air or Si-SiO_2 material combination offers a high index contrast material platform to realize PhC structures with large photonic band gap (PBG) and secondly, the fabrication process for Si is well established. However, strong nonlinear absorption, i.e. Two Photon Absorption (TPA) in Si adversely effects the performance of nonlinear Si photonic devices [18]. Recently, Silicon Nitride (Si_3N_4) is being exploited as an alternative material platform for nonlinear photonic applications [19]. Si_3N_4 platform offers several advantages, such as optical nonlinearity without any TPA for telecom wavelengths, large transmission window from visible wavelengths all the way to mid infrared wavelengths [20], CMOS compatible fabrication processes and possible 3D integration with other optical circuits. However, the nonlinear Kerr coefficient of Si_3N_4 is significantly lower than the corresponding value for Si. One way to improve the nonlinear coefficient is by increasing the Si content of the nitride film. Using such Si-Rich Nitride (SRN), different research groups have demonstrated enhanced nonlinear effects [21–24]. For example, Lacava et al. have demonstrated an order of magnitude improvement in nonlinear refractive index n_2 from $2.2\text{x}10^{-19}$ m^2/W for stoichiometric Si_3N_4 to $1.65\text{x}10^{-18}$ m^2/W with negligible increase in the TPA value [23]. Along with enhanced nonlinear effects, by controlling the Si content, the

Optics EXPRESS

refractive index of the SRN can also be increased. In this work, we demonstrate, to our knowledge for the first time, PhC waveguides in SRN membrane. First we present the design of SRN PhC structures and PhC waveguides with air holes. We then discuss the fabrication process that we developed to realize membraned SRN PhC structures. Finally we present the experimental characterization of the fabricated line defect PhC waveguides. We experimentally demonstrated group index over 110 and propagation loss of 53 dB/cm for group index of 37 for a W1 PhC waveguide. To realize broadband operation we used a W0.7 PhC waveguide, which showed a transmission band of over 70 nm and propagation loss of 4.6 dB/cm at group index of 7.4 in the fast light region.

2. Design and fabrication of SRN PhC waveguides

Due to the relatively low refractive index of SRN in comparison to Si, we first carried out a feasibility study of 2D PhC structure on SRN platform. Using three-dimensional plane wave expansion method (calculation was done using commercial software RSoft's Bandsolve package), we calculated the photonic band structure of a SRN 2D PhC slab. We used a 300 nm thick SRN film with a refractive index of 2.54. The PhC consisted of a hexagonal lattice of air holes with lattice constant a, as show in the inset of Fig. 1(a). The radius of air holes was set to $0.3a$. The calculated band diagram for the structure is shown in Fig. 1(a) for transverse electric (TE) polarization. The dotted line shows the light line of air, above which optical modes are leaky and will not be confined by the PhC slab. We found a clear PBG within the frequency range from $0.355(a/\lambda)$ to $0.44(a/\lambda)$. If the lattice period is chosen to be a = 580 nm, we can achieve a 210 nm wide PBG extending from 1320 nm up to1630 nm within the near infrared region.

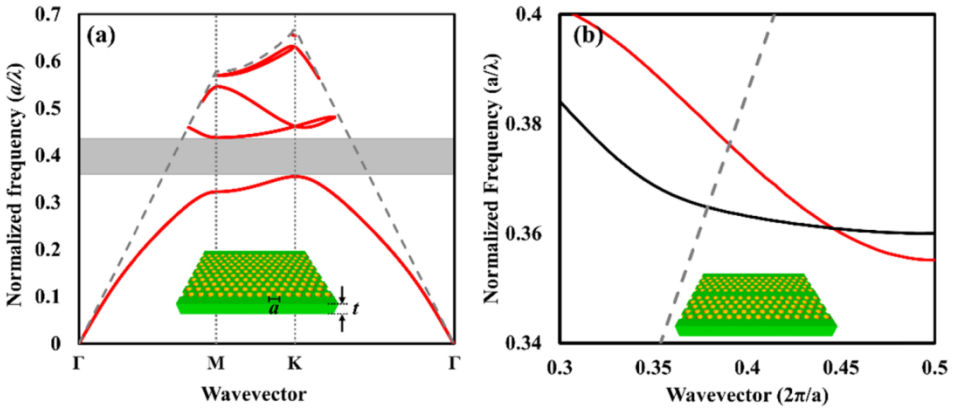

Fig. 1. (a) Photonic band diagram of triangular 2D PhC structure of air holes in SRN film, with refractive index of 2.54 and air hole radius of $0.3a$. The structure is shown in the inset with t = 300 nm. The PBG is shown in shaded region and the air light line is depicted using the dashed line. (b) Dispersion relation for a W1 and W0.7 slab waveguide shown in black and red respectively. The dashed line represents the air light line. By modifying the waveguide width transmission bandwidth can be increased from 20 nm to around 90 nm. The line defect waveguide structure is shown in inset.

For realizing waveguides in such PhC structure, we first created a line defect by removing a row of holes along Γ-K direction, as shown in the inset of Fig. 1(b), which is also called W1 waveguide. We again used the plane wave expansion method to calculate the dispersion relation for the waveguide along the direction of wave propagation. The dispersion relation is shown in black in Fig. 1(b). The dashed line represents the air light line. From this dispersion diagram the estimated band-width is around 20 nm and the photonic band edge lies at around 1595 nm. The transmission bandwidth is relatively low in comparison to Si-based PhC waveguides. This is due to relatively low index contrast of the SRN material. However, in

Optics EXPRESS

order to obtain a broader transmission bandwidth, the dispersion of the waveguide can be modified by adjusting the width of the waveguide. When the waveguide width is set to W0.7, this corresponds to waveguide width of 0.7 × sqrt(3) × a, the dispersion relation is shown in red in Fig. 1(b). For W0.7 waveguide the transmission bandwidth increases to 0.0206(a/λ), which corresponds to 90 nm bandwidth.

Figure 2 outlines the major fabrication steps used in this work to realize the PhC waveguides. A 300 nm thick SRN layer was deposited on a (100) bulk silicon wafer using SiH_4 and N_2 gases in a Plasma Enhanced Chemical Vapor deposition (PECVD) system at 350 °C. We used an optimized gas mixture of 3.6 sccm SiH_4 and 650 sccm N_2 to reduce the propagation loss at 1550 nm and also to achieve relatively high refractive index. A detailed analysis of such optimization process can be found in [25]. Using ellipsometry we confirmed the refractive index of the deposited film to be 2.54 at 1550 nm wavelength and the film thickness to be 300 nm. The substrate was then spin-coated with 450 nm thick layer of ZEP 520A, a positive ebeam resist. Using ebeam lithography, the desired patterns were exposed onto the ZEP layer. After developing the exposed resist layer using ZED-N50 developer, the patterns were transferred to the SRN layer in an inductively coupled plasma (ICP) etcher using SF_6/CHF_3 gas chemistry. After the dry etching process, the remaining resist was removed using an O_2 plasma asher. Final cleaning was carried out in fuming nitric acid (FNA) and diluted hydrofluoric acid (HF). Immediately after the HF cleaning process, the substrate was immersed in a 25% aqueous solution of Tetra-methyl-ammonium hydroxide (TMAH) which selectively etches Si through the exposed area. TMAH etching is very selective to the crystallographic orientation of the exposed Si surface. This was taken into account while designing the PhC waveguides, which allowed the successful realization of suspended structures. We also used a significantly long wet etching time to make sure that the effect of the substrate is minimum during the optical measurement.

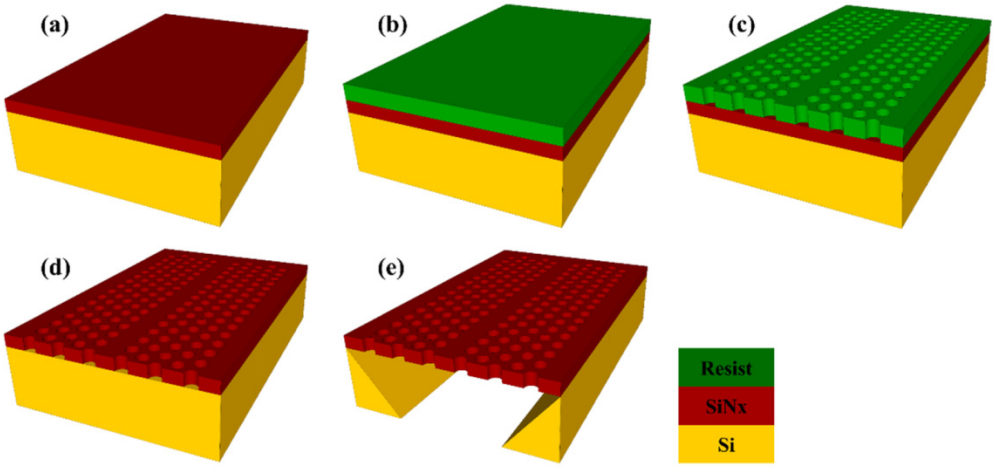

Fig. 2. The fabrication process flow of suspended PhC waveguide in SRN platform: (a) a 300 nm thick layer of SRN is deposited onto a bulk Si substrate using PECVD. (b) A 450 nm thick layer of ZEP 520A is spin coated onto the substrate, (c) Desired patterns were written on the resist using e-beam lithography, (d) patterns were transferred to the Si layer using ICP dry etching process, (e) SRN membrane is created by removing the exposed Si using TMAH solution with an etch depth of over 4 µm.

Figure 3(a) shows the optical micrograph of a set of fabricated PhC waveguides of different lengths along with a reference waveguide without any PhC region. We used grating couplers to launch light into the access waveguides, which are then coupled to the PhC waveguides. Figure 3(b) shows an SEM image of the coupling region between the access waveguide and the PhC waveguide. In order to achieve mechanical stability in the

Optics EXPRESS

freestanding access waveguide region we chose a subwavelength grating waveguide design, while making sure that the stop band for the structure is far from our operating wavelength region. The subwavelength structure has a period of 500 nm with 50% duty cycle. Figure 3(c) shows the cross-sectional view of the membraned PhC structure. From the cross-sectional view, we realized that the air holes were etched uniformly with vertical side walls. A zoomed in view of the PhC region, shown in Fig. 3(d), reveals that there is some surface roughness, which came from the deposition process. In order to quantify the surface roughness, we also performed atomic force microscopy, which suggest that the surface roughness is around 4 nm (rms value).

3. Measurements and Discussion

The transmission properties of the fabricated PhC waveguides were measured using a fiber coupler setup. Light from a tunable laser source, with wavelength range from 1530 nm to 1620 nm, is coupled to the waveguide using fiber-grating couplers. The laser wavelength was scanned using the built-in sweeping capability of the laser and the photodetector automatically recorded the output spectra. For all the measurements, we have used 10 dBm laser power. Since the PhC waveguides were designed for TE polarization, we ensured that only TE polarized light is launched into the waveguide by sending light through a fiber polarization controller. The grating couplers were designed with 1100 nm period and 50% duty cycle also to ensure that only TE polarized light is coupled to the waveguides.

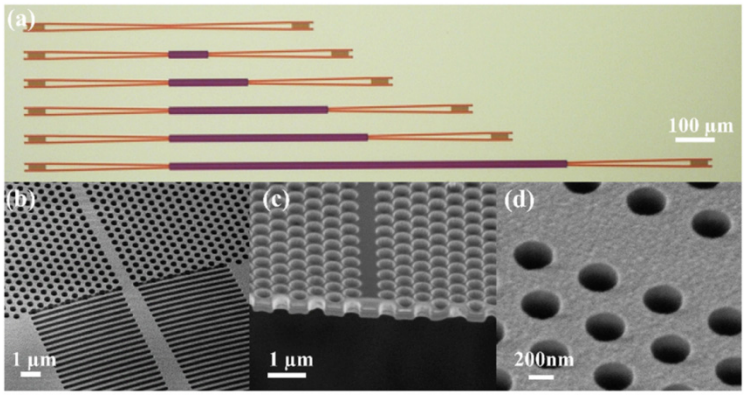

Fig. 3. (a) Optical image of the fabricated waveguides, (b) SEM image of the fabricated device, showing a part of the PhC waveguide coupled to the access waveguide. A subwavelength grating waveguide was used to increase the mechanical stability of the access waveguide. (c) Zoomed in view of the PhC structure showing the circular holes. And (d) shows the surface roughness arising from deposition process.

We have designed PhC waveguides with different lattice periods to lithographically tune the transmission spectra within the laser wavelength range. Figure 4 shows the transmission spectra for 100 µm long W1 PhC waveguides with period a = 560 nm, 570 nm and 580 nm and air hole radius of 170 nm. The recorded transmission spectra are shown in light colors and the trend in the transmission, which was obtained after filtering out the Fabry–Pérot oscillations using a causal moving average filter, is highlighted using dark colors. The Fabry–Pérot oscillations in the transmission spectra arise from the group index mismatch between the access waveguide and PhC waveguide at the coupling region. Also due to such index mismatch, the coupling efficiency between the access waveguide and the PhC waveguide reduces as the group index of the PhC waveguide increases. This poor coupling efficiency can be improved by incorporating a short coupling region, where the PhC waveguide is slightly stretched in the lateral direction [26, 27]. Besides, the low overall transmission is also due to the poor coupling efficiency of the grating couplers. From the transmission spectra, it can be

Optics EXPRESS

seen that the PBG for the PhC waveguide with a period of 580 nm starts around 1585 nm and, as expected, the reduction in the lattice period blue shifts the PBG. The extinction ratio at the PBG is around 20 dB. We see a 10 nm shift in the PBG cut-off position from the simulated value, which we believe is more likely due to slight variation in device parameters, such as stress induced in the suspended SRN layer, SRN thickness or refractive index, or the fabricated hole size.

Next, we investigate the transmission properties in details of the W1 PhC waveguide with lattice period of 580 nm. In Fig. 5(a) we plotted the normalized transmission curve in gray and the trend in transmission in black. The waveguide transmission is normalized by setting the background loss (i.e. setup and coupling loss) to 0 dB. Here we plotted the transmission spectrum of a 200 μm long waveguide. As a result, along with PBG, we also clearly observe a second cut-off appearing at a shorter wavelength, which corresponds to the air light line. The two cut-off regions are highlighted in the figure. The difference between the two cut-off wavelengths decides the operating bandwidth of the PhC waveguide. For the W1 waveguide the operating bandwidth is only about 20 nm.

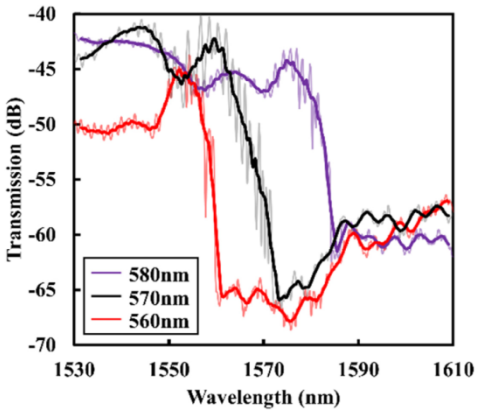

Fig. 4. Measured transmission spectra through 100 μm long PhC waveguides with lattice period a = 560 nm, 570 nm and 580 nm and air hole radius of 170 nm. The recorded transmission spectra are shown in light colors and the trends in the transmission, are highlighted using dark colors. Clear cut-offs corresponding to PBG with over 20 dB extinction ratio are visible.

As discussed in the introductory section, the main characteristic of PhC waveguides is the strong dispersion of their optical mode close to the PBG, which causes a monotonous increase in group index for a PhC waveguide. We calculated the group index for the waveguide from the dispersion relation of the waveguide using the expression: $n_g = c(\delta k/\delta\omega)$, where n_g is the group index, c is the velocity of light in vacuum, k is the wave vector and ω is the frequency. The calculated group index curve is shown in black in Fig. 5(b). We can also estimate the group index of the fabricated PhC waveguide by analyzing the Fabry–Pérot oscillation of the transmission spectrum. The Fabry–Pérot oscillation arises due to the cavity effect originating from the coupling region between the access waveguide and the PhC waveguide. The period of the Fabry–Pérot oscillation is directly related to the group index at a particular wavelength and the group index can be expressed as $n_g = \lambda^2/(2L\Delta\lambda)$, where λ is the operating wavelength, L is the length of the PhC waveguide and $\Delta\lambda$ is the difference between the two maxima around the operating wavelength. The estimated group indices are presented in Fig. 5(b) using green squares. Here we have only plotted the group index value up to the cut-off wavelength corresponding to the air light line, since beyond this point the waveguide mode becomes leaky. The calculated group index curve is shifted by 10 nm to overlap with the estimated group index values. The estimated group index values show a close match with the calculated group index curve. The highest group index that we measured was 110, which is comparable

Optics EXPRESS

to that measured for Si PhC waveguides [11, 12]. This suggest that SRN-based PhC waveguides can potentially replace Si PhC waveguides to achieve a similar kind of slow down effect. In Fig. 5(b) we also plotted the propagation loss of the W1 PhC waveguide at different wavelengths using red dots. We estimated the propagation loss using the cut-back technique. We used five different waveguide lengths ranging from 100 µm to 1 mm, as shown in Fig. 3(a) and by using linear regression we estimated the waveguide propagation loss at different wavelengths. As expected the propagation loss increases linearly with the group index. For example, at 1575 nm wavelength the group index is 37 and the propagation loss is 53 dB/cm, whereas at 1582 nm wavelength for a group index value of 100 the propagation loss increases to about 138 dB/cm.

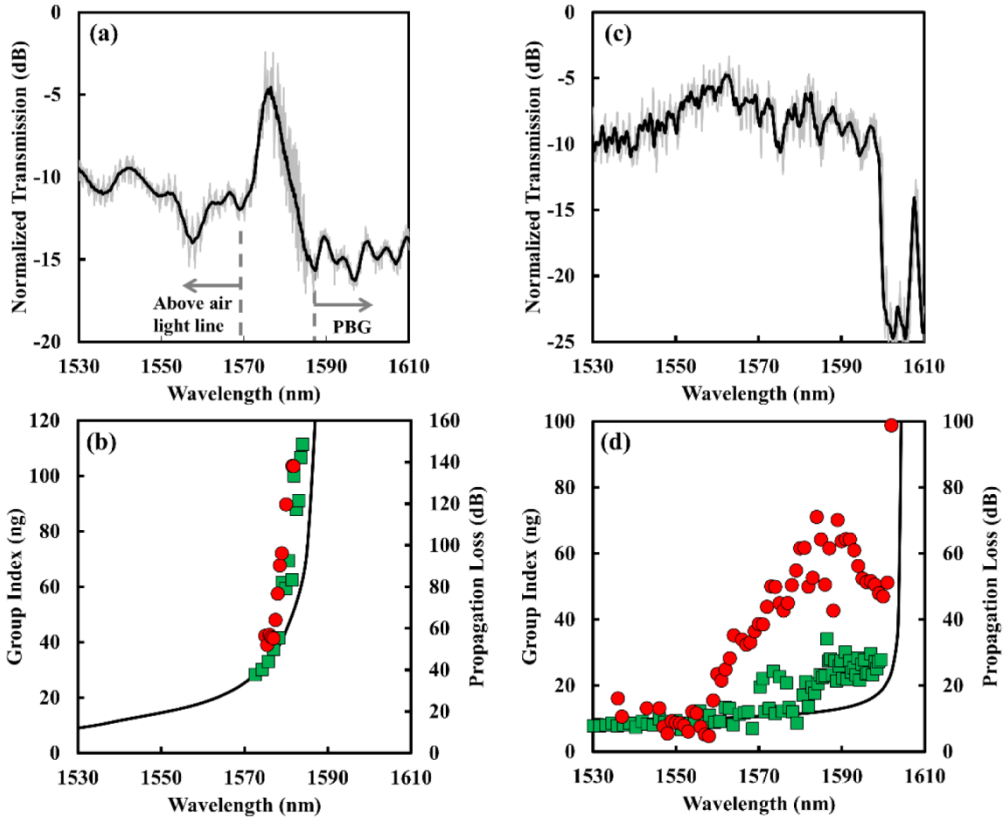

Fig. 5. W1 waveguide: (a) Gray and black curves show the measured transmission spectrum and the trend in transmission spectrum respectively for a 200 µm long waveguide with lattice period a = 580 nm. The transmission region is about 20 nm and highlighted by the dashed lines. (b) The calculated group index curve is shown in black and estimated group index values of the fabricated device is shown with green squares. The highest estimated group index is 110. The waveguide propagation loss is shown in red dots and the lowest propagation loss measured was 53 dB/cm for a group index of 37. W0.7 waveguide: (c) Gray and black curves show the measured transmission spectrum and the trend in transmission spectrum respectively for a 200 µm long waveguide with lattice period a = 580 nm. The transmission bandwidth is over 70 nm covering the entire laser tuning range. (d) The calculated group index curve is shown in black and estimated group index values of the fabricated device is shown with green squares. The highest estimated group index is 34. The waveguide propagation loss is shown in red dots and the lowest propagation loss measured was 4.6 dB/cm for a group index of 7.4.

Although, using W1 PhC waveguide, we managed to demonstrate high group index values, their low transmission bandwidth could cause serious drawbacks for any practical applications. As discussed in the previous section, one way to avoid such bandwidth

Optics EXPRESS

limitations is by reducing the waveguide width. Here we used a W0.7 PhC waveguide to demonstrate broadband operation. Figure 5(c) shows the transmission spectrum of a 200 μm long W0.7 PhC waveguide, where the measured transmission is shown in gray and the trend is shown in black. We can observe a clear cutoff at 1602 nm wavelength due to PBG and relatively flat transmission is observed within the tunable laser wavelength range. In Fig. 5(d), we plot the calculated group index curve in black and the estimated group index is plotted using green squares. The group index of W0.7 does not increase as high as W1 waveguide close to the PBG and the highest group index we could estimate from the Fabry–Pérot oscillations in the transmission spectra is 34. This is expected since the dispersion curve for W1 waveguide is flatter near the PBG in comparison to W0.7 waveguide, as apparent in Fig. 1(b). The propagation loss at different wavelengths is plotted using red squares. In the fast light region, the lowest propagation loss was 4.6 dB/cm for a group index value of 7.4 and as expected the propagation loss increases with group index. We believe that in our case the major factor to the propagation loss is surface roughness (as visible in Fig. 3(d). This can be avoided either by further optimization of the deposition process or by planarization using Chemical Mechanical Polishing (CMP).

4. Conclusion

To summarize, we have demonstrated PhC waveguides on SRN platform for applications in telecom wavelengths. The PECVD deposited SRN film had a refractive index of 2.54. Our theoretical calculation suggested that SRN-based PhC structures can have optical performance comparable to high index contrast materials such as Si. We successfully developed a fabrication process to realize suspended SRN structures on Si using a combination of dry and wet etching processes. Finally, we experimentally demonstrated W1 and W0.7 PhC waveguides with air holes in SRN. We observed clear bandgap with extinction ratio of over 20 dB for different PhC waveguide designs. For W1 waveguides we estimated group index of over 110, this value is quite comparable to Si based PhC waveguides. However, the main drawback of W1 waveguide is the transmission bandwidth, which is about 20 nm. By using a W0.7 waveguide we experimentally demonstrated large transmission bandwidth of over 70 nm. For W1 waveguide we estimated a propagation loss of 53 dB/cm for a group index of 37 and for W0.7 waveguide the lowest loss we measured was 4.6 dB/cm in the fast light region. With these results, we expect that our current demonstration will stimulate further research to develop PhC based devices on SRN platform, aiming for sensing and integrated nonlinear photonics applications.

5. Funding

This work was supported by the H2020 project COSMICC (688516), EPSRC Standard Grant (EP/M009416/1), EPSRC Manufacturing Fellowship (EP/M008975/1), EPSRC Platform Grant (EP/N013247/1), and EU FP7 Marie-Curie Carrier-Integration-Grant (PCIG13-GA-2013-618116).

Acknowledgement

All data supporting this study are available from the University of Southampton repository at: http://dx.doi.org/10.5258/SOTON/401736.